IRIS AperTO

UNIVERSITÀ DEGLI STUDI DI TORINO

AperTO - Archivio Istituzionale Open Access dell'Università di Torino

Tailored properties of hematite particles with different size and shape

This is a pre print version of the following article:

Original Citation:

Availability:

This version is available http://hdl.handle.net/2318/153534 since 2016-10-10T08:35:40Z

Published version:

DOI:10.1016/j.dyepig.2014.11.024

Terms of use:

Open Access

Anyone can freely access the full text of works made available as "Open Access". Works made available under a Creative Commons license can be used according to the terms and conditions of said license. Use of all other works requires consent of the right holder (author or publisher) if not exempted from copyright protection by the applicable law.

(Article begins on next page)

05 February 2025

Tailored properties of hematite particles with different size and shape

L. Demarchis[a,*], F. Sordello[a], M. Minella[a], C. Minero[a]

[a] *Department of Chemistry and NIS center of excellence, University of Turin, via Pietro Giuria 7, 10125, Turin (TO), Italy*

[*] Corresponding author: *E-mail address:* luca.demarchis@unito.it; *Phone:* +390116705298

Abstract

Cubic and spherical hematite red cool pigments with different size were synthesized following two different methods. Cubic and spherical particles with larger sizes were obtained through a gel-sol method using chloride and nitrilotriacetate as shape controllers, respectively, and changing the starting temperature to control the final particles size. Spherical particles with smaller sizes were synthesized in a faster way following a catalytic phase transformation method in which the size control is obtained by varying the reagent concentration. Cool properties for the obtained particles were evaluated by calculating the Solar Reflectance for all hematite samples. The cool properties differ depending on the particle size and shape. By controlling the final size and morphology of pigment particles it is possible to obtain pigments with the desired cool properties. Pigment color properties were also evaluated using CIE XYZ and CIE xyY color spaces.

Keywords: Hematite; Cool pigments; Solar Reflectance; Size control; Shape controlled particles

1. Introduction

The removal of natural vegetation and its replacement with buildings and paved surfaces [1] lead to an increase of temperature in urban city centers that in some cases can be also 10 °C higher than that of nearby rural places [2]. This phenomenon, called Urban Heat Island (UHI), has the effect of increasing the demand of energy (with a subsequent increase of energy supply costs), accelerating the formation of harmful smog and causing human thermal discomfort and health problems owing to the intensification of heat waves over cities [3-4].

Strategies for the mitigation of the UHI effects have been reported by Coutts et al. [5]. The development of new sustainable cities that use materials with high solar reflectance and thermal emissivity, the so-called "cool materials" has been proposed. Usually, cool materials are used to decrease the heat flow entering in a building. Their surface temperature is much lower than those of typical building materials and, if used on an urban scale, they help to decrease the air temperature of the urban environment reducing the harmful effects related to the UHI. Considerable interest has been directed to the roofing materials [6-9]. Among these, white materials are obviously effective. Coatings with colored conventional pigments tend to absorb solar light (both Vis and NIR radiation, which conveys more than 50% of the sunlight power) resulting in heat accumulation [10]. The replacement of these conventional absorbing pigments with "cool pigments", which absorb less NIR radiation, makes possible coatings with higher solar reflectance, but similar in color to that of conventional or old-style roofing materials. Cool colored coatings can then be applied on roofs, building envelopes and other surfaces of the urban environment, such as exterior finishes and paints, or they can be used to produce building materials that reflect more sunlight than conventionally pigmented products.

For this purpose, in recent years pigments of different colors with cool properties have been commercialized. The color features of pigment materials (one or more) depend on their visible

absorption, on their size (which varies scattering properties), and on their composition [11]. To tune the color properties of a material, pigments with different chemical composition are used.Sometimes, they contains environmental unfriendly metals such V and rare earths [12], or are toxic, containing Cd or Cr. The main proposed cool pigments contain inorganic complex pigments, such as chromium green, cobalt blue, cadmium stannate, lead chromate, cadmium yellow and chromium titanate [10, 13]. Among NIR reflective pigments with promising characteristics there are rare earth mixed oxides such as Me_xMnO_y (where Me = Y, Ce, Pr, Nd and Sm [12, 14]), or rare earth metals - molybdenum mixed oxides such as Y_6MoO_{12} [15]. Another approach is the use of pigments with particles coated with a metallic film [16]. The main drawback of the cool pigments obtained with both the described approaches is the high costs.

The choice of color depends on tradition and aesthetic needs, e.g. Italian traditional roofs are dark red, while in Thailand they are green. A database with optical characteristics of a huge number of pigments [17] is available to assist the optimization of the Solar Reflectance for industries which operate in the building sector. In the cited database there are four red pigments based on iron oxides.

In this work, we report the synthesis and investigation of hematite-based cool red pigments. It is known that for a given material (and for given optical constants) the optical properties depend on size, morphology and cluster aggregation of particles, so a set of syntheses was performed to obtain hematite particles with different size and shape. The optical properties of all the synthesized samples were analyzed with the aim to give insights into the relation between these properties and the morphological features of the pigment particles. We obtained different kinds of morphology suitable for cool pigment applications.

2. Materials and methods

76 *2.1 Materials*

77

78 The hematite particles were synthetized using (when needed) iron (III) chloride hexahydrate
79 (Sigma-Aldrich, > 99%), iron (II) chloride tetrahydrate (Fluka, > 99%), sodium hydroxide (Sigma-
80 Aldrich, > 99%), hydrochloric acid (Carlo Erba, 37%), nitrilotriacetic acid trisodium salt (Fluka, >
81 98%), sodium sulphate (Aldrich, > 99%) and sodium chloride (Carlo Erba, > 99,5%). For sample
82 washing, 1 M ammonia solution (Fluka, 25%) and 0.5 M sodium nitrate solution (Sigma-Aldrich, >
83 99%) were utilized. Ultra-pure water produced by a Milli-Q^{TM} system (Millipore) was used.
84 Commercial polyacetovinyl emulsion (Vinavil NPC, Vinavil SPA) was used as dispersing medium
85 for the preparation of paints.

86

87 *2.2 Hematite syntheses*

88

89 In literature several synthetic methods to produce hematite particles are reported [18-19 and
90 references therein]. In this work, monodisperse hematite particles with different size and shape have
91 been obtained following two different procedures.
92 The first, proposed by Sugimoto [20], is a gel-sol transformation procedure which produces
93 hematite particles starting from inexpensive ferric chloride. The process involves a two-step phase
94 transformation from concentrated $Fe(OH)_3$ gel via β-FeOOH (akaganeite) to α-Fe_2O_3 [21]. In the
95 standard procedure 45 mL of 6 M NaOH were slowly added to 50 mL of magnetically stirred 2 M
96 $FeCl_3$ solution. The slurry was then kept under stirring for additional 10 minutes. The obtained
97 $Fe(OH)_3$ gel was then transferred into a tightly stoppered bottle and heated at 100°C for at least 3
98 days until the conversion occurred.
99 The second synthetic method follows the catalytic phase transformation mechanism proposed by
100 Liu and co-workers [22], in which lower conversion times are attained by the addition of Fe(II) in

101 catalytic amount to the initial $Fe(OH)_3$ gel, lower conversion times are attained. The following
102 standard experimental procedure was followed: 6M NaOH was slowly added to 50 mL of a
103 magnetically stirred 2M $FeCl_3$ solution (unless for experiments in which [Fe(III)] was changed)
104 until pH 7 (typically ca. 49 mL). Then, $FeCl_2$ was added in the ratio [Fe(II)]/[Fe(III)] = 0.02 to the
105 gel and pH was readjusted to 7 adding dilute NaOH. The slurry was kept under stirring for
106 additional 10 minutes and then refluxed (for at least 30 minutes) until conversion to hematite
107 occurred.
108 The size of final hematite particles was modified by varying different experimental parameters such
109 as pH, temperature, reagents concentration and $FeCl_2$ amount.
110 Several anions have been shown to play a decisive role in the anisotropic growth of hematite
111 particles [23-24]. These shape controllers selectively adsorb on the surface of nuclei regulating the
112 growth of specific hematite crystal faces determining the final particle morphology. Several
113 syntheses were performed for both methods adding anions such as chloride, sulphate and
114 nitrilotriacetate to obtain hematite particles with pseudocubic, ellipsoidal and spherical morphology,
115 respectively. For this purpose, shape controllers 0,05 M were added to the initial gel of iron
116 hydroxide before the heat treatment.
117 After heat treatment, all the as-prepared hematite samples were washed with ultra pure water three
118 times, once with 1 M NH_3 and three times again with ultra pure water. The pigments were separated
119 from the supernatant with centrifugation at 1370 g. Then each sample was dried at 70°C.
120
121 *2.3 Hematite characterization*
122
123 The crystalline phase of the samples was identified with X-Ray Diffraction and Raman analyses. X-
124 ray powder diffraction (XRD) patterns have been recorded with a PW3050/60 X'Pert PRO MPD
125 diffractometer from PANalytical working in Bragg-Brentano configuration. The X-ray source was a

high power ceramic tube PW3373/10 LFF with a Cu anode and the instrument was equipped with a Ni filter to attenuate Kb. Diffracted photons were collected with a real time multiple strip X'celerator detector. Powder samples have been hosted on SiO_2 amorphous sample holder. Raman spectroscopy analyses were performed with a LABRAM HRVIS (Jobin Yvon), fitted with an Olympus BX41 optical microscope. Raman spectra were excited using the 533 nm line of a Nd solid state laser. The laser power was 100 mW. Spectra were collected over the range 80–1525 cm^{-1} at a resolution of approximately 2 cm^{-1}.

Size and shape of synthesized hematite particles were determined through scanning electron microscopy by a Scanning Electron Microscope Zeiss model EVO-50 XVP operating at 15 kV, beam current 50.0 μA, probe intensity 50 pA.

2.4 Optical properties evaluation

Total reflectance analyses were carried out to determine scattering properties of the samples using a dual-beam Varian Cary 5000 UV-VIS-NIR Spectrometer with an integrating sphere. The internal walls of the sphere are coated with Polytetrafluoroethylene (PTFE) and $BaSO_4$ was used as reference material. Light sources are a deuterium lamp in the 185–350 nm range and a halogen lamp in the 350-3300 nm range. The detection is performed by means of R928 PMT (185–800 nm) and Cooled PbS (800–3300 nm) detectors. The analyses were performed over the range 200-2500 nm. To estimate the solar reflectance (*SR*) of obtained hematite, the total reflectance data were weighted on solar irradiance data for each sample following the equation:

$$SR = \frac{\int_{280}^{2500} P_{solar}(\lambda) \bullet R(\lambda)}{\int_{280}^{2500} P_{solar}(\lambda)} \quad (1)$$

148 in which $P_{solar}(\lambda)$ is the AM 1 solar irradiance [25]; $R(\lambda)$ is the measured total (diffuse and specular)
149 reflectance for the investigated material. *SR* varies from 0 to 1, for a total absorptive and total
150 reflective material, respectively, and represents the capability of reflecting sunlight; the higher it is,
151 the better will be the cool properties for the investigated material.
152
153 *2.5 Color evaluation*
154
155 Color measurements were performed using tristimulus analysis and the CIE XYZ 1931and CIE xyY
156 color spaces.
157 Analyses were performed recording reflectance spectra and elaborating data by means of Ocean
158 Optics "SpectraSuite" software. Reflectance analyses were carried out using a Micropack ISP-50-8-
159 R-GT integrating sphere connected to the light source and to the detector with optical fibers.
160 Irradiation was performed using a Micropack DH-2000 UV-Vis-NIR Lightsource and the detection
161 by means of an Ocean Optics USB2000 detector. A Micropack $BaSO_4$ standard was used as
162 reference. Analyses were carried out on paints with a load of ca. 3% in weight of pigments. Paints
163 were prepared dispersing 0.12 g of pigments in 1 ml of ultra-pure water by sonication for 30
164 minutes; then 3 g of commercial polyacetovinyl emulsion were added to the system and additional
165 sonication for 30 minutes was performed. Some drops were then poured on white and black
166 paperboards and spread using a metallic filmographer, obtaining films of about 250 μm of
167 thickness. Paints were first dried for 15 minutes in air and then at 75°C for 15 minutes.
168
169 **3. Results and discussion**
170
171 *3.1 Shape and size control*
172

Figure 1 and Figure 2 show XRD patterns and Raman spectra for a selection of the pigments synthesized; similar results were obtained for all the other pigments. Analyses were carried out on samples obtained following the two synthetic procedures with different morphology and size. In both XRD and Raman analyses, all signals are relative to α-Fe_2O_3 phase, indicating that pure hematite particles were obtained. Both XRD and Raman also indicate that no other crystalline phases are formed.

Figure 3 and Figure 4 show SEM micrographs for synthesized particles in the presence of shape controllers. In the case of the catalytic phase transformation procedure, it was not possible to obtain shape control and all the samples showed a spherical morphology. Instead, different kinds of particle morphology were obtained in the case of gel-sol method. Accordingly to literature data [23-24], pseudocubic (Figure 4a), ellipsoidal (Figure 4b) and spherical-ovoidal (Figure 4c) particles are obtained by adding chloride, sulphate and nitrilotriacetate, respectively.

The different ability of these anions as shape controllers as a function of the adopted synthetic method can be explained considering the different heat treatments and conversion rates in the two methods. The catalytic phase transformation syntheses show high conversion rates and turbulent motions are present in the system during the treatment. These two events hinder the attainment of adsorption equilibrium of shape controllers on the surface compromising the anisotropic growth of hematite nuclei, and yielding only spherical particles. Instead, in the gel-sol procedure the synthesis was carried out in quiet and the conversion rate was low: hematite nuclei can grow regularly and the effect of shape controllers can be maximized.

Results also show that for both synthetic methods, obtained particles show quite uniform size; only in the case of addition of sulphate in the gel-sol method is size inhomogeneity observed. Using the reported synthetic methods it was possible to obtain large quantities of hematite particles with different shapes with uniform size distribution, necessary for the study of the relation between particle morphology and SR.

198 The particles size control for both gel-sol and catalytic phase transformation method can be
199 obtained varying the experimental conditions. In the case of gel-sol preparations, an appreciable
200 variation of the final particles size is obtained varying the temperature of the system in the initial
201 step of addition of NaOH to $FeCl_3$. Temperature influences the nucleation rate of iron hydroxide;
202 increasing the temperature, a higher amount of nuclei is formed and subsequently smaller hematite
203 particles are obtained.
204 Figure 5 shows the final particle diameter as a function of the synthesis temperature demonstrating
205 that hematite particles can be synthesized in a wide range of size, from 500 to 1300 nm. Other
206 syntheses were performed varying other parameters such as pH or the synthesis temperature in the
207 presence of Fe(II) ions, but no appreciable effect on the final size of the particles was observed
208 (figures S1, S2 and S3 of the supporting information, hereafter SI).
209 With the catalytic phase transformation method of synthesis, size control can be obtained tuning the
210 concentration of $FeCl_3$. Increasing the amount of iron chloride, bigger particles are obtained thanks
211 to the higher amount of iron suitable for the growth of hematite particles (Figure 6).
212 The particles are always lower in size (100 - 400 nm) compared to those obtained with the gel-sol
213 method. This is due to the turbulent motions occurring during the heating step which limit the size
214 of the final particles. Other parameters, such as Fe(II)/Fe(III) ratio, pH and initial temperature were
215 investigated, but no appreciable changes in the final size were observed (see figures S4, S5 and S6
216 of SI).
217
218 *3.2 Optical properties evaluation*
219 Figure 7 shows the total reflectance spectrum of a synthesized hematite sample (other samples show
220 DR spectra with similar features, see figures S7 and S8 of SI). The materials synthesized show
221 absorption in the Visible part of the spectrum and reflectance > 50% above 1000 nm and >75%

above 1300 nm, being therefore promising candidates for cool applications, since high NIR reflectance is coupled to hematite coloristic properties.

Using reflectance data (%R) and eq.(1), SR for hematite samples was calculated. Figure 8 shows SR as a function of particle shape and size. For particle size lower than 600 nm, cubic morphology shows the best SR values compared to spherical particles, whereas spherical hematite samples show best cool properties for particle size larger than 600 nm. SR of cubic particles shows two maxima, the first is a local maximum at particle size ca. 300 nm and the second at ca. 920 nm after which SR decreases rapidly. For spherical particles, SR shows a similar trend but with the local maximum at particle diameter ca. 250 nm and the second at ca. 600 nm. Note that, SR for the commercial cool red pigment Ferro V-13810 is 0.316, calculated with eq.(1) and the pigment spectrum provided by the producer [26]. SR values of as-synthesized hematite pigments are very close to that value and in some cases even larger.

Solar reflectance evaluation was also performed on paints for both white and black paperboards (see figures S9-S15 of SI for reflectance spectra and SR). Since the paints are not completely opaque in the NIR, the SR values are higher for paints on white paperboard compared to paints on black paperboard, with discrepancy up to 50%. Light scattering and absorption by paperboards interfere on the reflectance leading to unreliable results. With white papers the light is more scattered yielding to overestimated SRs, while black paperboards lead to undervalued results because of the absorption of the transmitted light. More studies will be performed to obtain completely opaque paints in order to evaluate correctly their SRs.

3.3 Color evaluation

In the visible range light paints are quite opaque and the results obtained for paints spread on white paperboards are not significantly different from those of paints on black papers. Table 1 shows the

247 results obtained from the analysis of paints on black paperboards (for white papers see table S1 of
248 SI), while in Figure 9 the color properties of the samples synthesized are reported in a portion of the
249 chromaticity diagram. Paints with spherical hematites show a quite constant chromaticity, except
250 for the sample with the largest particle size that shows lowest values for both x and y. For paints
251 with cubic particles x decreases increasing the size (from ca. 0.5 to ca. 0.39) while y remains
252 constant around 0.35. In both cases, a decrease of brightness (Y) increasing the size is observed. A
253 color variation from light orange-red to dark red-purple occurs increasing the pigment particle size.
254

255 **4.Conclusions**

256

257 Red cool pigments made of iron oxides can be obtained following two different procedures: *i*) a gel-
258 sol synthesis and *ii*) a catalytic phase transformation method which should be preferred in industrial
259 application because of the reduced time of synthesis. A fine tuning of the pigment particles size and
260 shape was obtained varying the temperature, the reagent concentration and by adding proper shape
261 controllers. As the optical properties of a pigment depend not only on the crystalline phase, but also
262 on the morphology of its particles, by varying size and shape of synthesized hematite we maximized
263 solar reflectance. The highest SR values were recorded with cubic particles with size 300 and 900
264 nm or spherical particles with size 250 and 600 nm. Size and shape of pigments also influence their
265 coloristic features; increasing the size of hematite particles darker color is obtained.
266 In conclusion, cool red materials for the mitigation of urban heat island can be obtained with
267 harmless inorganic pigments, synthesized from inexpensive precursors. Four different kinds of
268 hematite pigments which maximize SR, but with slightly different color properties, were obtained.
269

270 **Acknowledgement**

271

This research was supported by Rockwood Italia S.P.A. which financed Luca Demarchis' Ph. D. project.L. D. is thankful to the Photonic Resonance Department of the State University of Saint Petersburg for the help in the analyses.

Higlights

Development of pigments for the mitigation of Urban Heat Island effects.

We synthesized hematite particles with different size and shape.

We evaluated Solar Reflectance of hematite samples as a function of particle size and shape.

Color of pigments varies as a function of morphology.

Tables

Table 1: x, y and Y values for synthesized hematite pigments as functions of particles size

Spherical			
Dimensions (nm)	**x**	**y**	**Y**
128	0.471	0.354	11.3
147	0.472	0.348	10.6
229	0.459	0.341	8.53
270	0.459	0.341	8.38
446	0.455	0.344	7.68
583	0.446	0.340	6.98
1687	0.390	0.334	5.25
Cubic			
Dimensions (nm)	**x**	**y**	**Y**
250	0.492	0.356	8.18
307	0.492	0.356	8.28
536	0.438	0.344	5.74
708	0.425	0.348	5.14
921	0.447	0.355	5.86
989	0.424	0.354	4.85
1277	0.411	0.361	4.59
1478	0.392	0.358	4.47

288 **Figures**

289

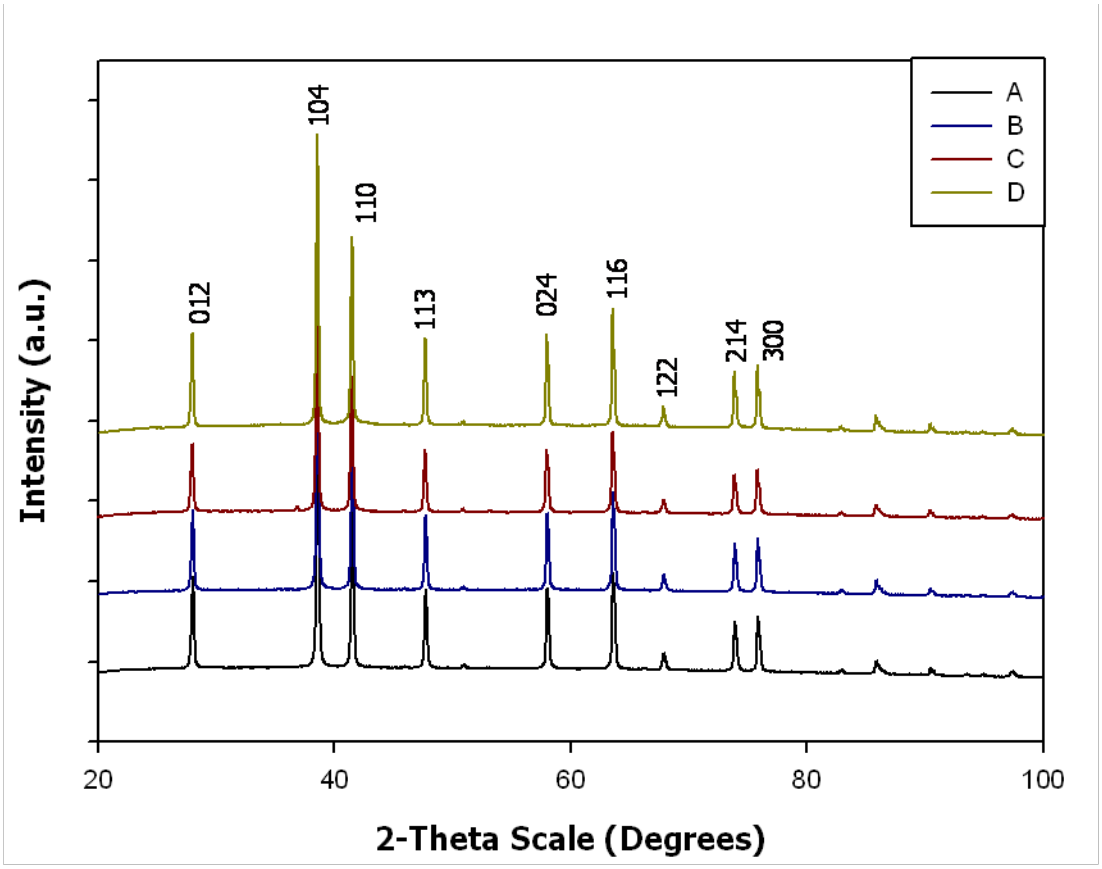

290

291 Figure 1

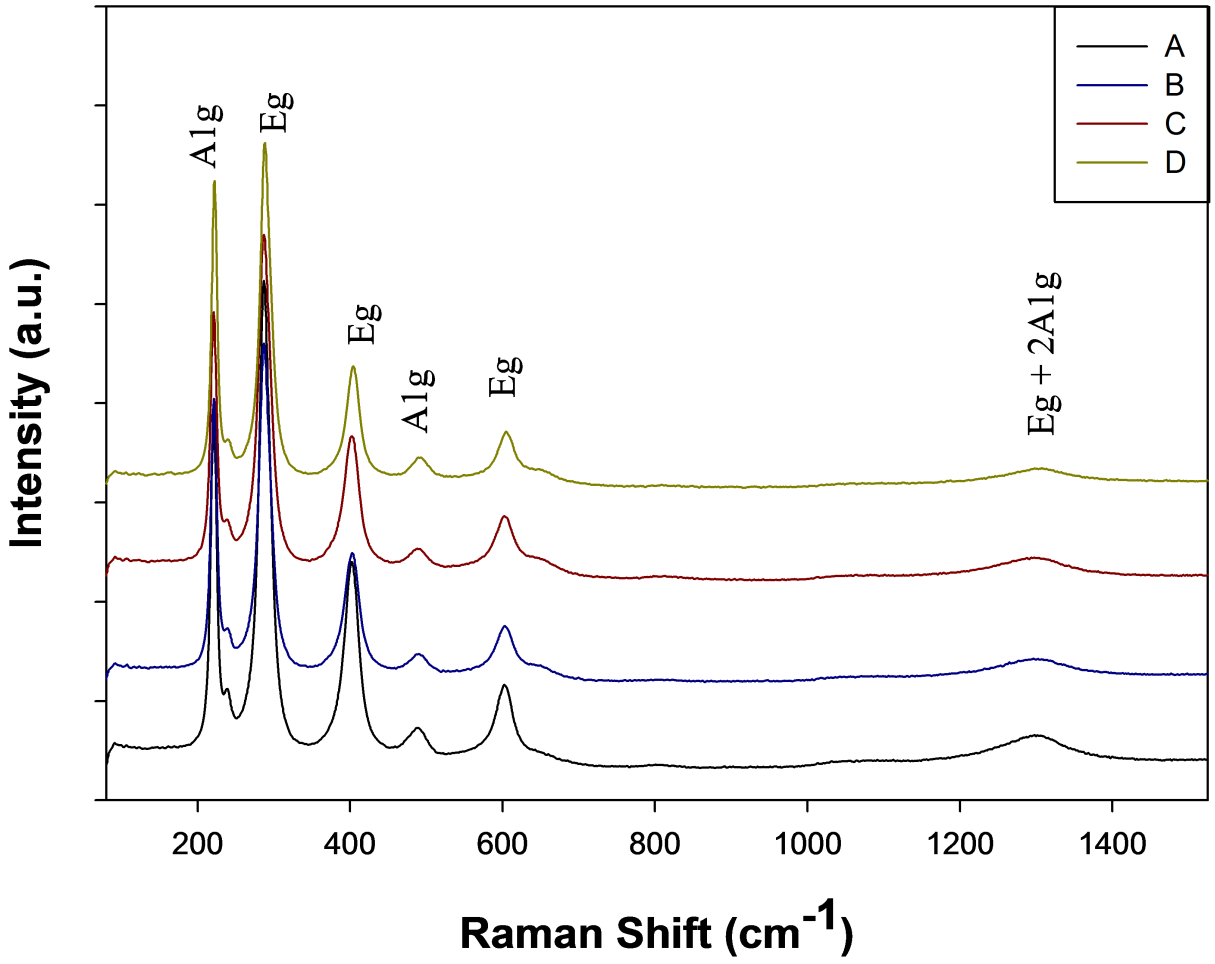

292

293 Figure 2

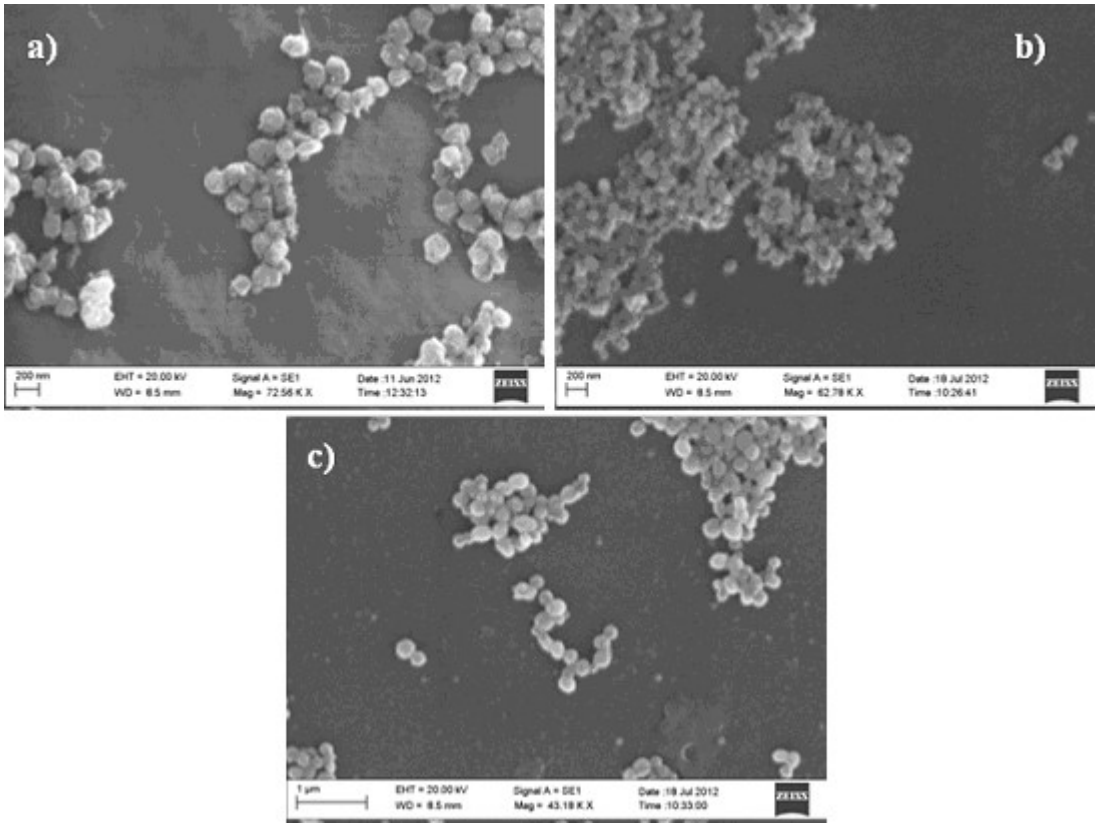

294

295 Figure 3

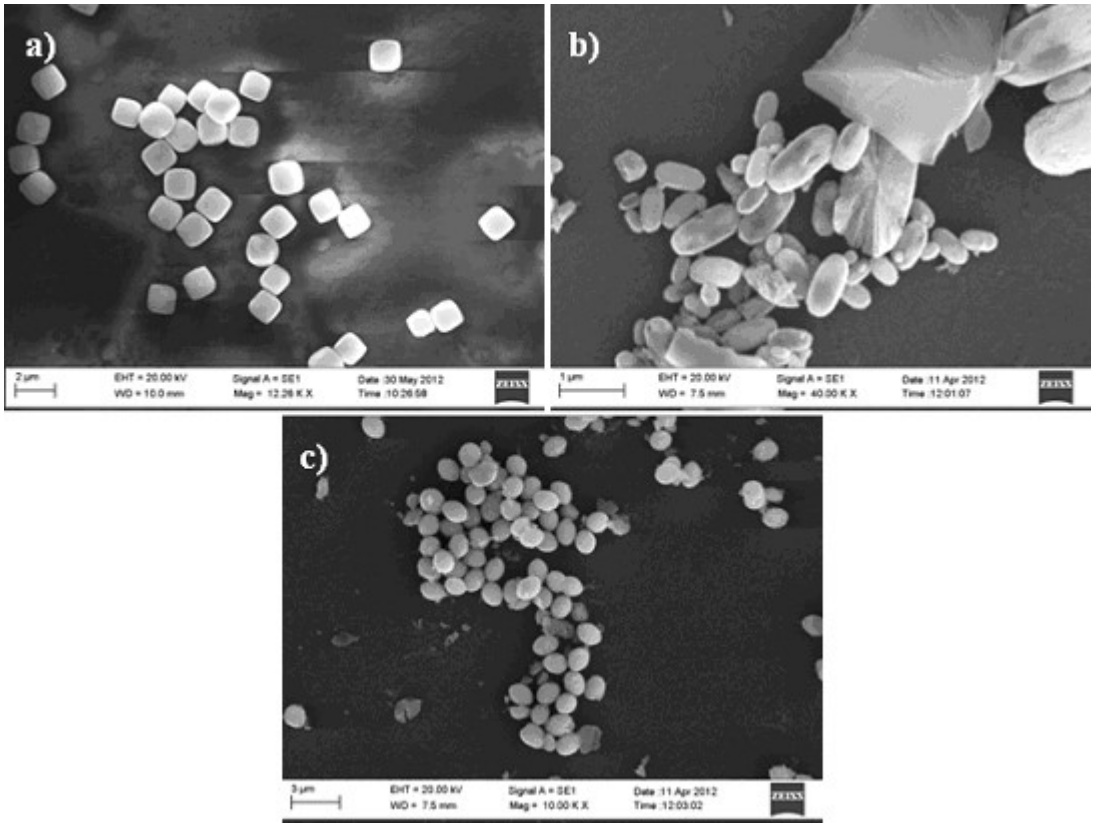

296

297 Figure 4

298

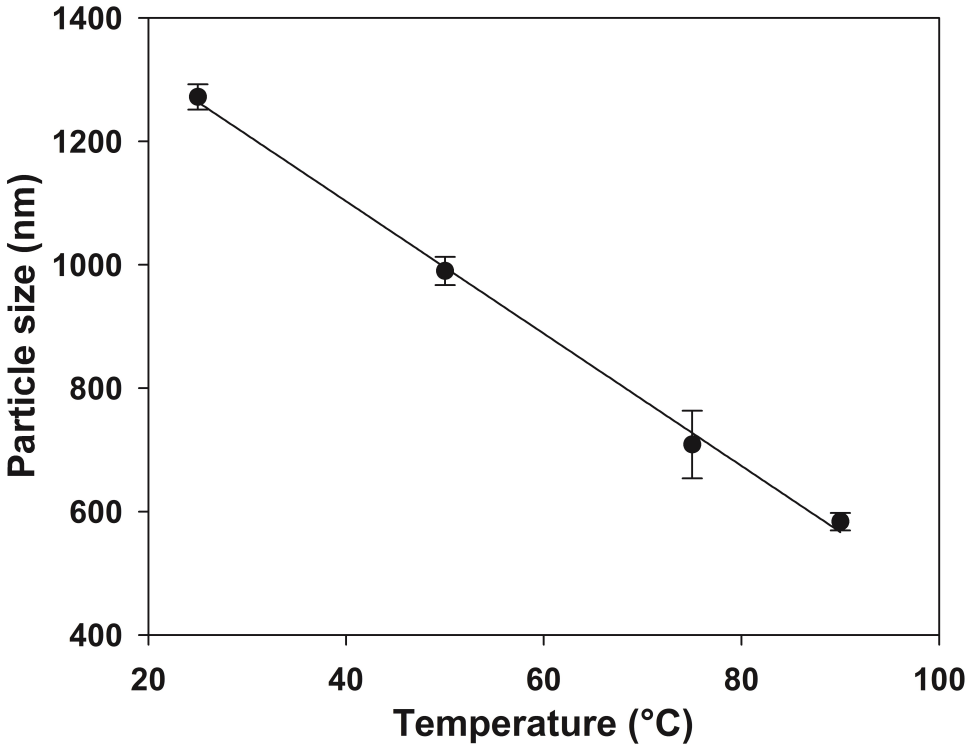

299

300 Figure 5

301

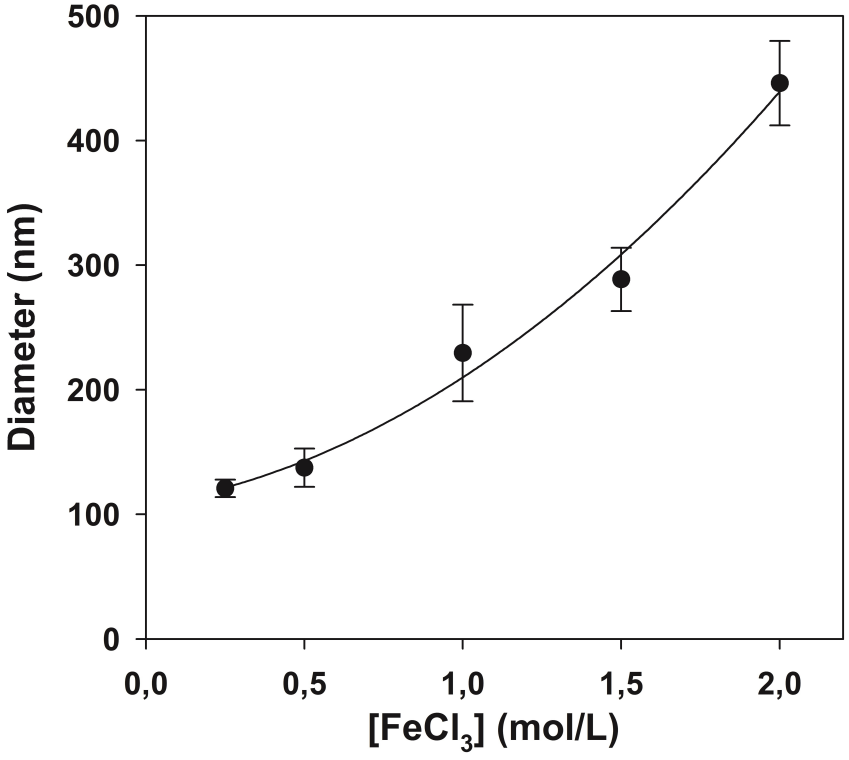

302

303 Figure 6

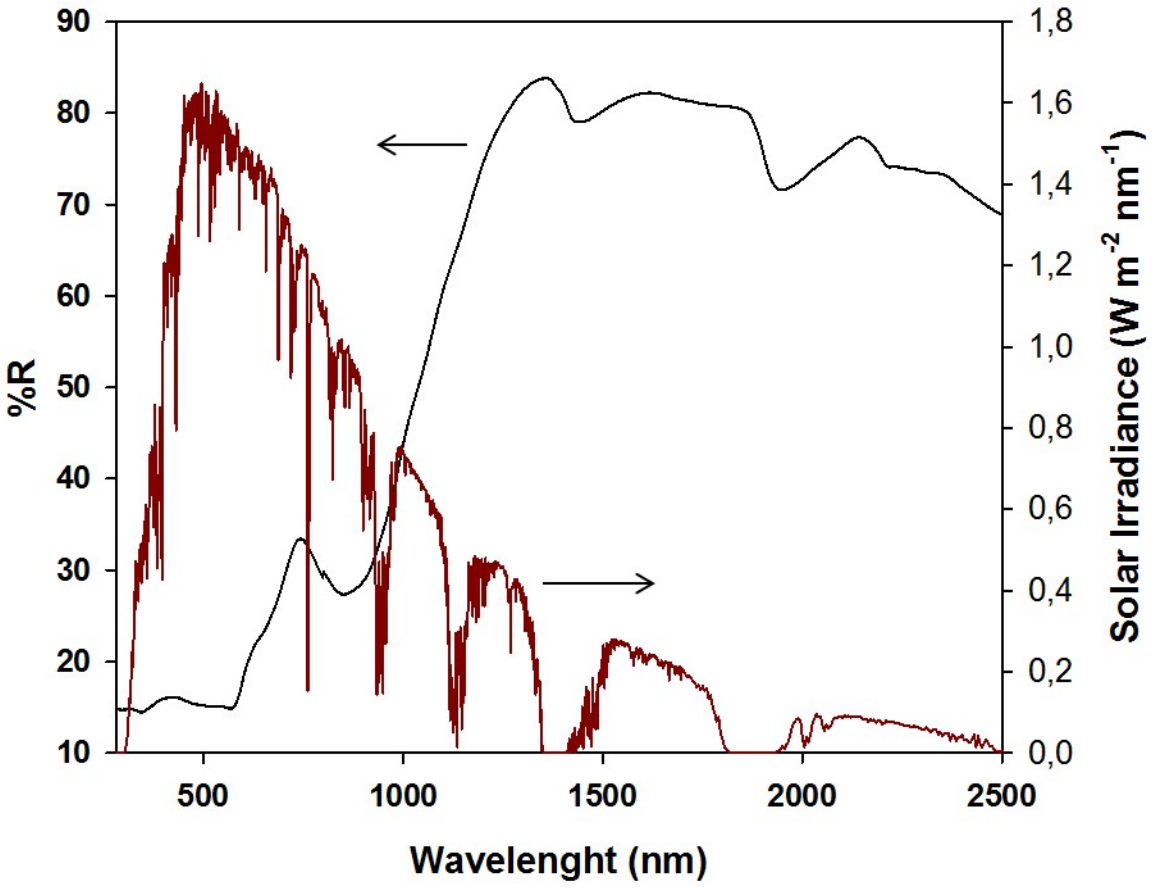

304

305 Figure 7

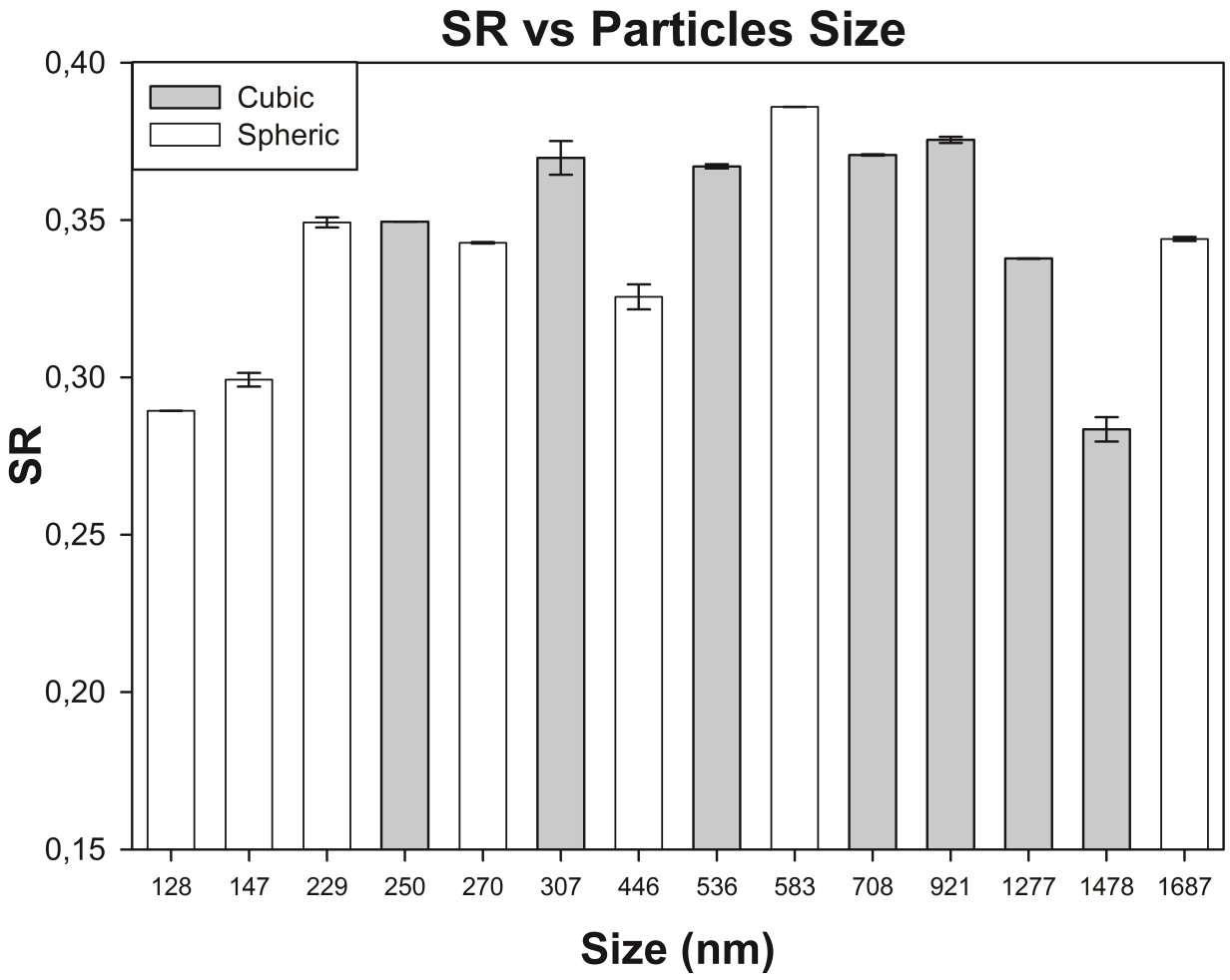

306

307 Figure 8

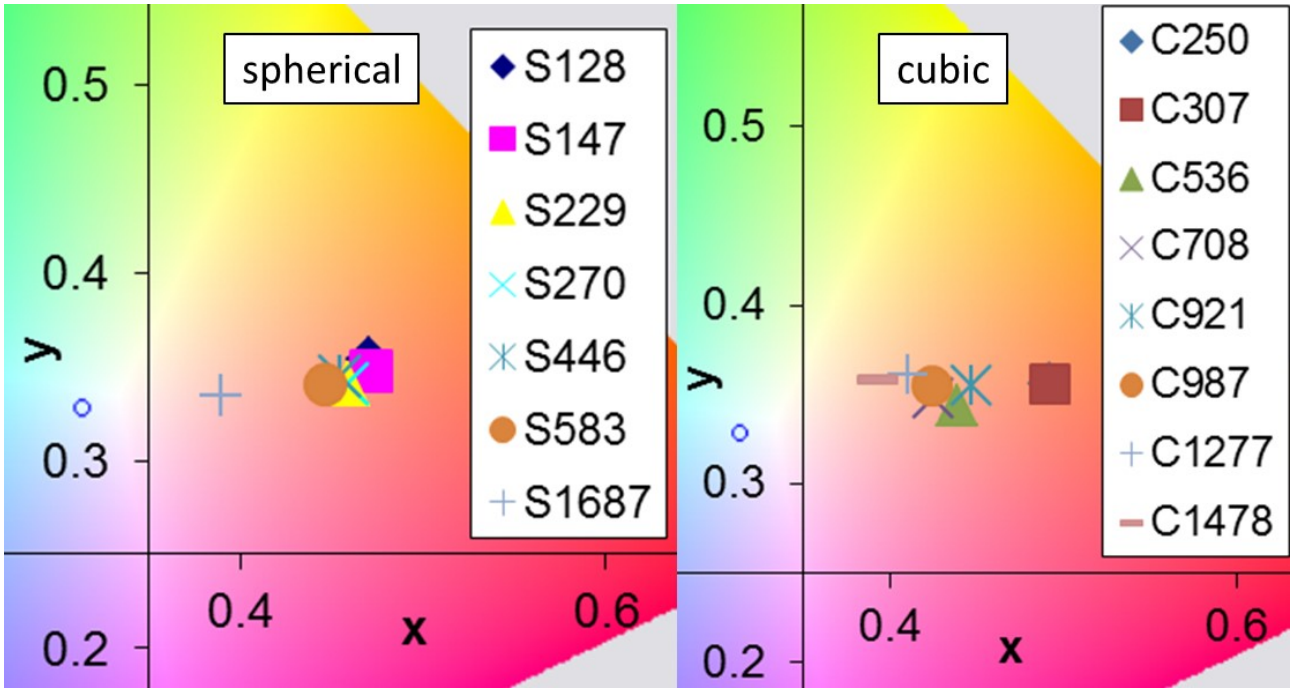
spherical
S128
S147
S229
S270
S446
S583
S1687
0.5
0.4
0.3
0.2
y
0.4
x
0.6
cubic
C250
C307
C536
C708
C921
C987
C1277
C1478
0.5
0.4
0.3
0.2
y
0.4
x
0.6

Figure 9

Captions to figures

Fig. 1.. X-Ray Diffraction patterns for four different hematite samples. Samples A and B were obtained following the gel-sol procedure and show spherical and pseudocubic morphology, respectively, with an average size of 1000 nm. Samples C and D were obtained via the catalytic phase transformation method; they are both spherical with an average size of 100 and 300 nm, respectively.

Fig. 2.. Raman spectra of four different synthesized hematites. Samples A-D have the same meaning as in Figure 1.

Fig. 3. Scanning electron micrographs for hematite particles obtained via catalytic phase transformation method with a) no shape controllers, b) chloride and c) nitrilotriacetate.

Fig. 4.. Scanning electron micrographs for hematite particles obtained via gel-sol method with a) chloride, b) sulphate and c) nitrilotriacetate.

Fig. 5. Diameter of hematite cubic particles obtained via gel-sol method as a function of the initial temperature. Chloride were used as shape controller. Other parameters were as indicated in the method reported in paragraph 2.2.

Fig. 6. Diameter of spherical hematite particles obtained via catalytic phase transformation method as a function of $FeCl_3$ concentration. Other parameters were as indicated in the method reported in paragraph 2.2..

Fig. 7. Solar irradiance (red) [25] and total reflectance (black) spectra of synthesized cubic hematite particles (1500 nm size, obtained via gel-sol synthetic method, chloride was used as shape controller, temperature 25°C. Other parameters were as indicated in the method reported in paragraph 2.2.).

Fig. 8. Solar Reflectance for hematite particles as a function of their size and shape.

Fig. 9. Plots on CIE color space chromaticity diagram of x and y values of prepared hematite paints. S and C mean spherical or cubic morphology, respectively, while numbers indicate particle dimensions.

334 **References**

335

336 [1] Synnefa A, Santamouris M, Apostolakis K. On the development, optical properties and thermal
337 performance of cool colored coatings for the urban environment. Solar Energy 2007;81(4):488-97.
338 [2] Uemoto KL, Sato NMN, John VM. Estimating thermal performance of cool colored paints.
339 Energy Build 2010;42(1):17-22.
340 [3] Cartalis C, Synodinou A, Proedrou M, Tsangrassoulis A, Santamouris M. Modifications in
341 energy demand in urban areas as a result of climate changes: an assessment for the southeast
342 Mediterranean region. Energy Convers Manage 2001;42(14):1647-56.
343 [4] Santamouris M, Papanikolaou N, Livada I, Koronakis I, Georgakis C, Argiriou A, et al. On the
344 impact of urban climate on the energy consumption of buildings. Solar Energy. 2001;70(3):201-16.
345 [5] Coutts A, Beringer J, Tapper N. Changing Urban Climate and CO_2 Emissions: Implications for
346 the Development of Policies for Sustainable Cities. Urban Policy Res. 2010;28(1):27-47.
347 [6] Hildebrandt EW, Bos W, Moore R. Assessing the impacts of white roofs on building energy
348 loads. Proc ASHRAE Transactions1998. p. 810-8.
349 [7] Akbari H, Bretz S, Kurn DM, Hanford J. Peak power and cooling energy savings of high-albedo
350 roofs. Energy Build. 1997;25(2):117-26.
351 [8] Parker DS, Huang YJ, Konopacki SJ, Gartland LM, Sherwin JR, Gu L. Measured and simulated
352 performance of reflective roofing systems in residential buildings. Proc ASHRAE
353 Transactions1998. p. 963-75.
354 [9] Sleiman M, Kirchstetter TW, Berdahl P, Gilbert HE, Quelen S, Marlot L, et al. Soiling of
355 building envelope surfaces and its effect on solar reflectance - Part II: Development of an
356 accelerated aging method for roofing materials. Sol Energy Mater Sol Cells. 2014;122:271-81.
357 [10] Levinson R, Berdahl P, Akbari H. Solar spectral optical properties of pigments—Part II:
358 survey of common colorants. Sol Energy Mater Sol Cells. 2005;89(4):351-89.

[11] Thongkanluang T, Limsuwan P, Rakkwamsuk P. Preparation and using of high near-infrared reflective green pigments on ceramic glaze. J Ceram Soc Jpn. 2010;118(1377):349-52.

[12] Sreeram KJ, Aby CP, Nair BU, Ramasami T. Colored cool colorants based on rare earth metal ions. Sol Energy Mater Sol Cells. 2008;92(11):1462-7.

[13] Jeevanandam P, Mulukutla RS, Phillips M, Chaudhuri S, Erickson LE, Klabunde KJ. Near infrared reflectance properties of metal oxide nanoparticles. J Phys Chem C. 2007;111(5):1912-8.

[14] Swiler DR, Detrie TJ, Axtell EA. Rare earth transition metal oxide pigments. US Patent2003.

[15] George G, Vishnu VS, Reddy MLP. The synthesis, characterization and optical properties of silicon and praseodymium doped Y_6MoO_{12} compounds: Environmentally benign inorganic pigments with high NIR reflectance. Dyes Pigm. 2011;88(1):109-15.

[16] Sutter CR, Petelinkar RA, Reeves RE. Infrared reflective visually colored metallic compositions. US Patent2002.

[17] Levinson R, Berdahl P, Akbari H. Lawrence Berkeley National Laboratory Pigment Database: http://coolcolors.lbl.gov/LBNL-Pigment-Database/database.html; last access: 2014-10-17.

[18] Cornell RM, Schwertmann U. The Iron Oxides: Structure, Properties, Reactions, Occurences and Uses. 2nd ed: Wiley, 2003.

[19] Mohapatra M, Anand S. Synthesis and applications of nano-structured iron oxides/hydroxides – a review. International Journal of Engineering, Science and Technology. 2010;2(8):127-46.

[20] Sugimoto T, Sakata K. Preparation of monodisperse pseudocubic α-Fe_2O_3 particles from condensed ferric hydroxide gel. J Colloid Interface Sci. 1992;152(2):587-90.

[21] Sugimoto T, Sakata K, Muramatsu A. Formation Mechanism of Monodisperse Pseudocubic α-Fe_2O_3 Particles from Condensed Ferric Hydroxide Gel. J Colloid Interface Sci. 1993;159(2):372-82.

[22] Liu H, Wei Y, Li P, Zhang Y, Sun Y. Catalytic synthesis of nanosized hematite particles in solution. Mater Chem Phys. 2007;102(1):1-6.

383 [23] Itoh H, Sugimoto T. Systematic control of size, shape, structure, and magnetic properties
384 of uniform magnetite and maghemite particles. J Colloid Interface Sci. 2003;265(2):283-95.
385 [24] Sugimoto T, Wang Y, Itoh H, Muramatsu A. Systematic control of size, shape and internal
386 structure of monodisperse α-Fe2O3 particles. Colloids Surf, A. 1998;134(3):265-79.
387 [25] Tables for Reference Solar Spectral Irradiances: Direct Normal and Hemispherical on 37 Tilted
388 Surface. ASTM International; 2012.
389 [26] Ferro WebSite. http://www.ferro.com/NR/rdonlyres/616CDD4C-1D20-4BFF-BF6E-
390 7C0863AE4151/2902/V13810TDS.pdf; last access: 2014-10-17.